RESEARCH ARTICLE

Bidirectional Synchronous H6 Inverter for Hybrid AC/DC Distribution System With Improved Light Load Efficiency

MESHARI ALSHAMMARI[1,2,3] AND MAEVE DUFFY[1,2], (Senior Member, IEEE)

[1]Power Electronics Research Centre, School of Engineering, University of Galway, Galway, H91HX31 Ireland
[2]Ryan Institute, University of Galway, Galway, H91HX31 Ireland
[3]Electrical Engineering Department, Faculty of Engineering, Jouf University, Sakaka 72388, Saudi Arabia

Corresponding author: Meshari Alshammari (m.alshammari2@nuigalway.ie)

ABSTRACT The overall efficiency of DC distribution systems may be impacted by the operation of the bidirectional inverter connected to the grid; one of its most critical components. When compared to high-demand industries, the typical load profile of such system in residential buildings is highly variable, including several periods of light-load. Therefore, this paper presents a method to overcome the reduced efficiency at light-load of bidirectional inverters integrated into a DC distribution system powered by renewable energy. Existing topologies are evaluated for obtaining optimal efficiency as well as an investigation of loss breakdown at light-load using analytic models and PSIM simulation. A novel synchronous H6 transformerless topology is proposed. Simulation results show that the proposed topology can achieve an efficiency of 96.5% under full load and 98.3% under light-load. Efficiency improvements over a standard H6 topology are 4.5% under light-load and 1.5 % at full load. This is mostly due to reduced conduction and switching ON loss of MOSFETS used to replace diodes. When using the rectifier mode, similar levels of improvement are observed, with a 4% increase under light-load and a 1.2% improvement under full load conditions, respectively. Experimental results confirm the effectiveness of the proposed topology, showing nearly the same trend in improvement vs. the standard H6.

INDEX TERMS Bidirectional inverter, DC system integration, grid interference, synchronous H6, light-load efficiency.

I. INTRODUCTION

In recent years, DC distribution systems have grown in popularity due to their superiority over standard AC systems in terms of improving overall efficiency in buildings, particularly when renewable energy sources are integrated [1]. When the AC system is replaced with the DC system, studies have shown that a relative reduction in system loss of up to 2.3% [2] and an improvement in grid energy savings of 7% [3] may be obtained. The advantage of the DC system may vary based on geographical location, allowing renewable energy sources to contribute to matching the load demand of

The associate editor coordinating the review of this manuscript and approving it for publication was Dinesh Kumar.

individual end-users throughout different seasons. For example, according to a study of the usage of the DC distribution system, [4] it reduces system losses by up to 50% in comparison to an equivalent AC distribution system and allow for an additional 5% decrease in grid energy consumption per year. DC distribution systems require the usage of bidirectional inverters because of their capability for dual-mode operation (see Figure 1): feeding the grid in the case of a surplus of PV power and drawing power from the utility grid in order to keep the DC bus operating at a nominal voltage when the load demand is higher than the PV supply.

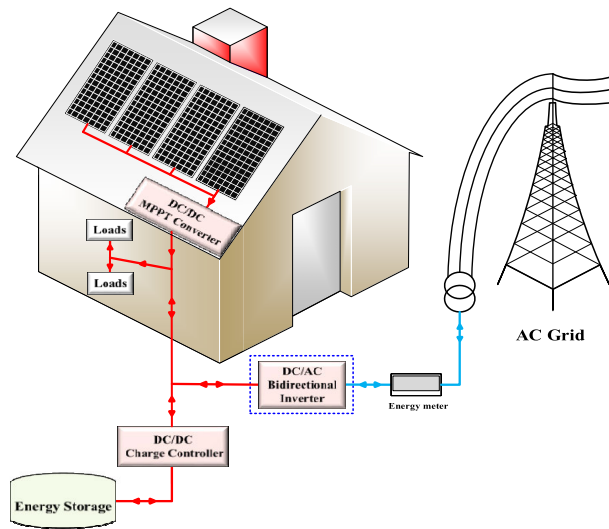High efficiency for light-load conditions is rarely studied, despite the abundance of research on the optimal performance of bidirectional inverters integrated with DC distribution

systems. Evidence from prior research shows that bidirectional inverters operate most efficiently under relatively high loads (> 20%). While commercial buildings often experience fairly consistent load levels throughout the day and year, residential buildings have much more erratic load patterns. Therefore, while a bidirectional inverter must be sized for maximum operational power, the varying seasonal load profiles show that the system operates at less than 20% of its maximum operational power for more than 70% of the time [5].Therefore, the efficiency of the system under light-load has a significant impact on the system's overall energy efficiency. In order to improve the efficiency of DC systems as a whole, this research analyzes the losses in a previously established H6 topology and proposes a new solution to improve the efficiency of the system under light-load.

Bidirectional inverters are required for a variety of applications, including Plug-in Electric Vehicles (PEVs) and energy storage systems (ESSs). Most high-power bidirectional converters used a two-stage topology with a DC-link capacitor due to its simplicity, and the benefits given by isolating the grid from the used on board battery charger of EVs [6], [7]. Similarly, a two stage topology operates as a bidirectional inverter between the EV motor and battery whether the battery is being charged or the motor is being supplied to drive the EVs [8], [9]. When considering ESSs such as rechargeable batteries or ultra-capacitor systems, they should be able to provide rapid frequency control, load monitoring, and system enhancement capabilities [10], [11], [12]. Despite the fact that in most circumstances, only a unidirectional rectification mode is required to charge the EV battery, it is probable that bidirectional capability will be required in EV applications to facilitate V2G between the grid and DC-bus.

However, the requirements for the bidirectional inverter for the aforementioned applications is different from those for residential/commercial use. Included in these requirements

are charging/discharging characteristics for the battery and safe operation when integrated with the utility. In addition, it is claimed that the efficiency of a transformer-based topology using two stages is limited in these cases [13], [14], [15], [16].

A transformer-less bidirectional inverter is most widely used in grid-connected PV installations due to the lower cost, smaller component size and higher efficiency compared to transformer based topologies [17]. However, the dynamic coupling between AC and DC sides of many transformer-less topologies causes a common mode (CM) voltage and leakage current flowing through a parasitic capacitance of the PV to ground [18], [19], [20]. The trade off between common mode voltage (CMV) and leakage current was shown in [21], and the ground impedance is a critical factor in defining this relationship. If the ground impedance is significantly high, no leakage current occurs, and the CMV is consequently at its maximum in this case. The leakage current is high when thesystem is firmly grounded, but there is no CMV, which implies that the system is not securely grounded. Leakage current may also be caused by high frequency PWM, and the scope for reducing it with lower operational frequency is limited by the need for larger filter components [22]. This view is supported in [23] who assess the most efficient transformer-less topologies when the PV and grid share the same ground to eliminate leakage current, specifically under inversion mode. Similarly, an interleaved high frequency leg (HFL) inverter was presented to reduce high current ripple and minimize switching losses under light-loads [24].

For bidirectional capability inverters, the full-bridge (H4) transformer-less design is the most widely used in renewable energy applications, as shown by [25], [26] for example. The usage of a modified H4 topology with an EMI filter to reduce high-frequency unipolar PWM leakage current on the AC filter is also proposed by [22]. The efficiency provided by the H4 topologies is not as high as it might have been partly a result of the ac filter structure, which results in extra loss. Thus, in [27] a high efficiency variation of the H4 transformer-less inverter with PFC is proposed in which a freewheeling path is introduced to overcome the leakage current issue. It is noted that the demonstrated efficiency was achieved using oversized MOSFETs and neglecting the effects of the output capacitor. Using an active common-mode duty cycle injection approach [28], a control solution for grounded systems with power converters is provided.

Control of the DC and low-frequency CMV is required to deliver a consistent bus voltage whilst also efficiently minimizing the effects of ground leakage current on the bus voltage. According to [29], the proposed topology should allow different operational input and output voltage ranges as well as high-frequency operation. The use of CMV decoupling also resulted in a reduction in leakage current, while a filter was used to remove high-frequency noise. Furthermore, an interleaved design of this topology was presented to prevent choke inductor ripple, which could lead to additional loss and low efficiency. Since this topology requires additional
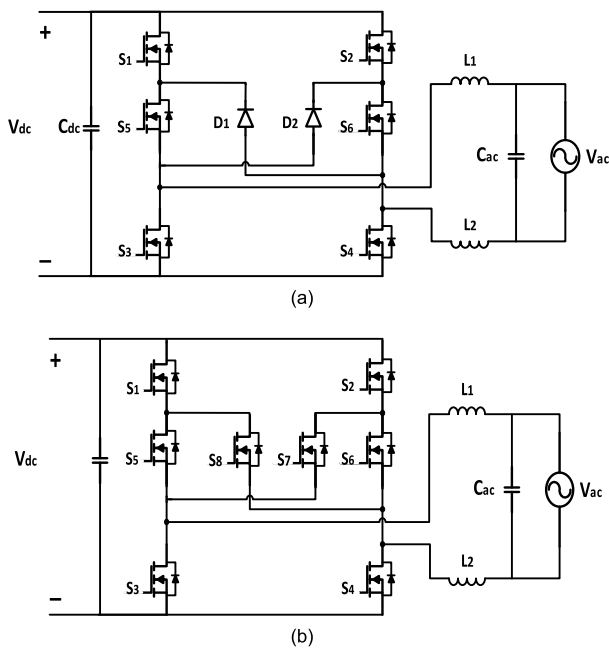
FIGURE 2. Circuits diagram of bidirectional inverter topologies of (a) Standard H6 [32] and (b) the proposed synchronous H6.

FIGURE 3. Pules width modulation for inverter mode.

switching devices and passive components, it is expected that the total system cost and size, would increase to achieve reactive power regulation.

Alternatively, a new H6 transformer-less inverter topology has been presented [30] that eliminates the leakage current, reduces inductor harmonic currents and reduces the voltage spikes that occur with inductive loads. Its efficiency was improved when a phase-shift was introduced between output current and voltage, and its bidirectional capability was modified [31]. A further development let to bidirectional capability modifying the switching pattern for S5 and S6 [32]. Due to additional semiconductor driving circuitry, the efficiency of the H6 perhaps reduces under low power level conditions (1.2 kW for a 5 kW nominal system). However, the features of the H6 still outweigh other transformer-less topologies such H5, HERIC, etc. by a large margin and therefore it was chosen as a benchmark design in this work. A summary of bidirectional inverters used for DC distribution system in buildings is presented in [33].

This study builds upon our previous work in [34], which proposes a modified synchronous version of the standard H6 topology in order to improve the topology's efficiency under light-load. In this paper, the literature review is updated to include the most current relevant literature. More detailed simulation results are presented to highlight the difference in performance between the standard and proposed synchronous H6 circuits. Finally, an extensive set of experimental findings is provided to support the performance of the proposed synchronous H6 inverter over the standard H6 inverter.

An illustration of the proposed topology is shown in Figure 2 (b). At light-load, switching and conduction losses of
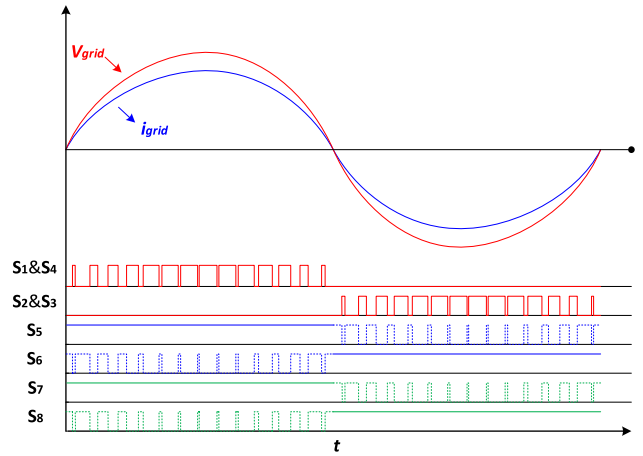
the diodes dominate, according to an analysis of the breakdown of losses in the standard H6 inverter [34]. As a result, the synchronous H6 topology has been proposed. In this topology, controlled MOSFETs S7 and S8 are used in place of diodes D1 and D2 which were utilized in the standard H6 topology to ensure that the inductor current remained continuous.

In the remainder of the paper, Section II describes the operating principle and control techniques of the proposed bidirectional synchronous H6 inverter. This includes modulation schemes, operation modes and associated control methods. The analysis and design considerations for the synchronous H6 including the selection of components and their associated power losses are presented in Section III. Section IV presents the experimental findings that validate the modelled results as well as the performance of the proposed synchronous H6. Finally, Section V provides concluding remarks of this work.

II. OPERATIONAL PRINCIPLE
The operation is the same as a standard H6 except that switches S7 and S8 need to be controlled so that they operate at the correct times to maintain continuous inductor current during the freewheeling interval.

A. MODULATION STRATEGY
The Pulse Width Modulation (PWM) signals of the diode replaced switches (S7 and S8) for the synchronous H6 are the inverse signals of S2 & S3 and S1 & S4 respectively. The PWM signals of S1-S4 have the same operating state as the standard H6. Figure 3, shows the modulation for inverter mode, where the line frequency is applied to switches S7 & S8 in this mode. The modulation method of the rectifier mode is illustrated in Figure 4. It is observed that a high frequency pulse is operated to turn on S7 & S8 in rectification mode due to the residual current from the former dead time state for both positive and negative cycles. The high frequency pulses are valid for both inversion and rectification modes, which can share the same drive signal for both modes.
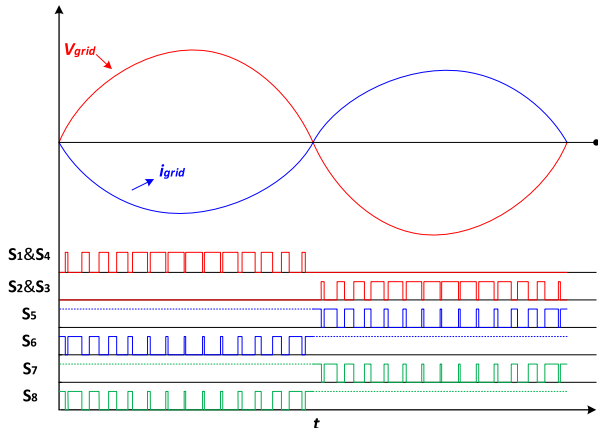
FIGURE 4. Pules width modulation for rectifier mode.

B. BIDIRECTIONAL SYNCHRONOUS H6 INVERTER OPERATION

1) INVERTER MODE (A)

The inverter operational modes are depicted in Figure 5. Figure 5 (a) shows the first mode during the positive grid cycle period where S1 & S4 are on, and S6 is off. S5 is on for the positive grid cycle to maintain continuity of the current flow when S1 and S4 are on.

2) INVERTER MODE (B)

In this second mode of the positive grid cycle, S1 and S4 are off, S5 & S7 are on all the time, and S6 & S8 are on enabling inductor current flow through two paths as shown in Figure 5(b). Thus, IL1 and IL2 are charged by the grid. The on state of S5 and S6 leads to sharing of the input voltage between S1 & S3 and S2 & S4, respectively.

3) INVERTER MODE (C)

Similarly, for the period of negative grid cycle, S2 & S3 are on, and S6 turns on maintaining the continuity of the current flow shown in Figure 5 (c).

4) INVERTER MODE (D)

S2 and S3 are off and the inductor current (IL1 and IL2) flows through two shared paths; S5 & S7 and S6 & S8 all of which are on. As a result, the input voltage will be split between S1 & S3 and S2 & S4 respectively.

C. BIDIRECTIONAL SYNCHRONOUS H6 RECTIFIER OPERATION

1) RECTIFIER MODE (A)

The rectifier operational modes are shown in Figure 6. Figure 6 (a) shows the first mode, where S1 & S4 are on and S5 and S6 are off. The inductor current (IL and IL2) will continue to flow thought S7 which is on, enabling current flow though the body diode of S2.

2) RECTIFIER MODE (B)

During this second mode, S1 and S4 are turned off, S5 and S7 are on, and S6 and S8 are on, enabling the current flow
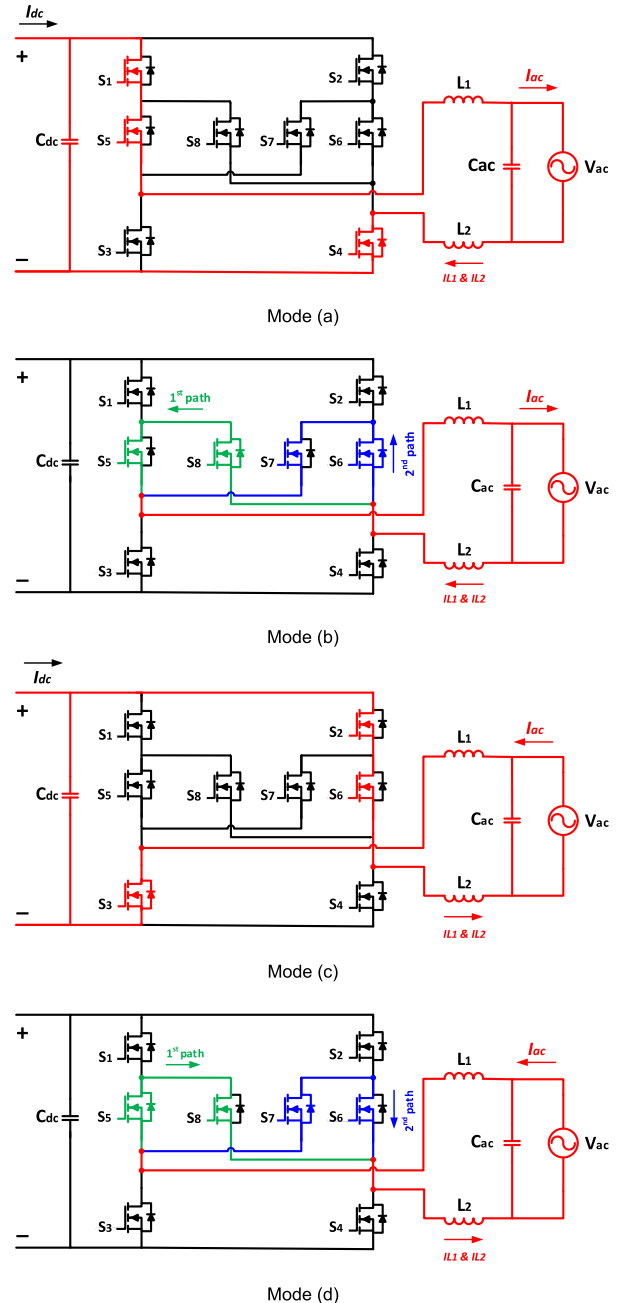

FIGURE 5. Inversion modes of synchronous H6.

through two paths as shown in Figure 6 (b). Thus, IL1 and IL2 are charged by the grid, with the on state of S5 and S6 resulting in sharing the input voltage between S1 and S3 and S2 and S4, respectively.

3) RECTIFIER MODE (C)

Similarly, for the period of negative grid cycle, S2 & S3 are on and S5 and S6 turn on as illustrated in Figure 6 (c). However, due to the residual current from the previous state, the inductor current (IL1 and IL2) will continue to flow through S8 which turns on, enabling the current though the body diode of S1.
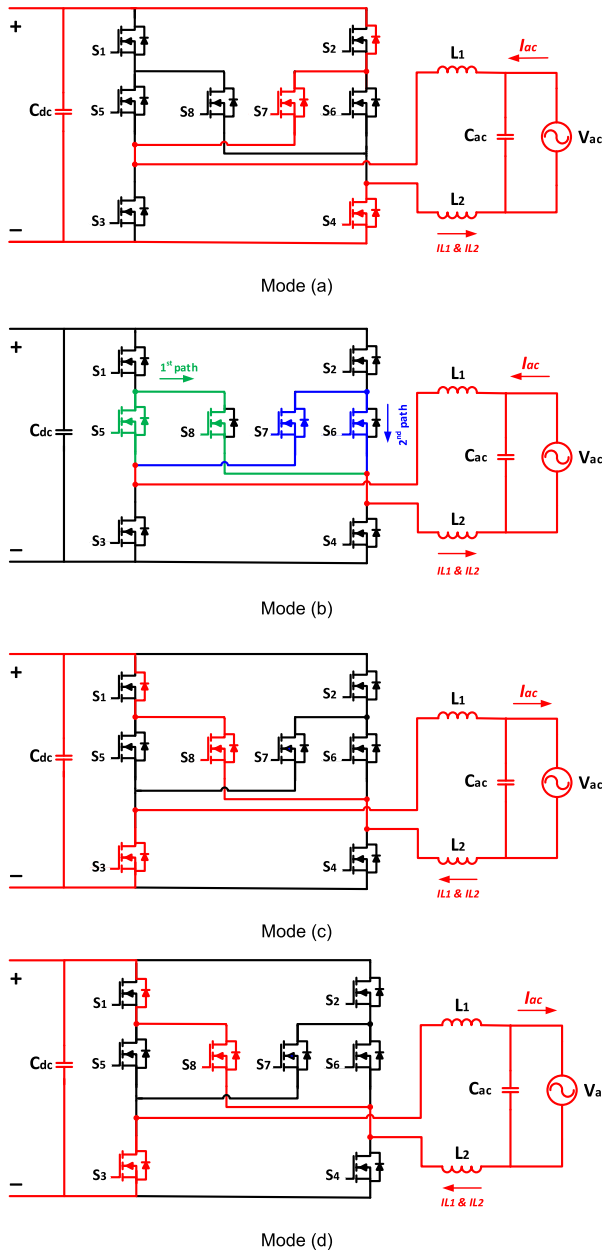
Mode (a)

Mode (b)

Mode (c)

Mode (d)

FIGURE 6. Rectification modes of synchronous H6.

4) RECTIFIER MODE (D)

S2 and S3 are turned off and the inductor current (IL1 and IL2) flows though shared two paths during the open state; S5 & S7 and S6 & S8 all of which are on. Consequentially, the input voltage will be divided between S1& S3 and S2 & S4 in a corresponding manner.

D. MODULATION COMPARISON BETWEEN BIDIRECTIONAL STANDARD AND SYNCHRONOUS H6 INVERTER

A comparison between the standard and synchronous H6 topology is shown in Table 1. It is noticeable that the operating modes of the H6 inverter when using the proposed
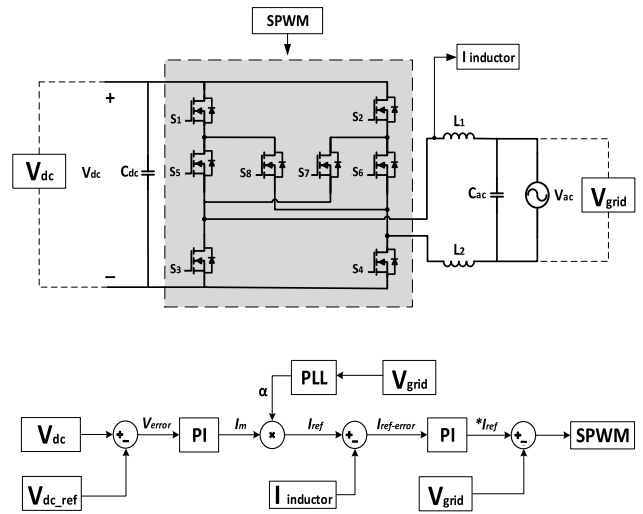

FIGURE 7. Block diagram of the control strategy.

modulation method (Synchronous H6) is approximately similar to the operation of the standard H6. However, Figure 3 illustrates the differences between the switching patterns of the switches that have replaced diodes D7 and D8 (S7 and S8). In fact, the switching patterns for both the S7 and the S8 are identical to the switching patterns for S5 and S6 respectively. Similarly, switching pulses for S7 and S8 may also be used in rectifier mode, as seen in Figure 4 (b). As a result, modulation strategies for both modes should be the same and should not be adjusted while switching modes.

Although there is a contrast between the two figures, high frequency switching pulses are employed in S5-S8 for rectifier mode in the first half of the mains cycle, while line frequency switching pulses are used in S5-S8 for the second half of the mains cycle, as illustrated in Figure 4 (a) and (b). It is worth noting that the body diodes of (S1, S2) are employed in rectifier mode, though they are not used in inverter mode in both standard and synchronous circuits, as shown in the preceding section. In the case of the inverter mode, however, the body diode of the replacement switches (S7 & S8) is used during the freewheeling path, whereas their body diodes are always used in the rectifier. It is believed that the body diode of S7 and S8 has an effect on the efficiency of the synchronous H6 circuit while it is operating in the rectification mode.

E. BIDIRECTIONAL SYNCHRONOUS H6 CONTROL METHOD

The proposed synchronous H6 topology's control strategy is depicted in Figure 7. In order to achieve the desired active and reactive power and ensure the system's stability, two variables must be controlled in a grid-connected topology such as the output current and voltage. Thus, the DC-bus voltage is controlled by a voltage control loop. Using the PLL block, the output value is instantly synchronized with the grid voltage by multiplying it by the grid current Im generated at this stage, which is proportional to the grid voltage.

TABLE 1. A summary of the comparison between standard and synchronous H6.

Figure	Mode	Current Paths		V_{cm}	V_{dm}
		Standard H6	Synchronous H6		
Fig 5(a)	Inverter mode (a)	S_1, S_5, L_1, grid, L_2 and S4	S_1, S_5, L_1, grid, L_2 and S4	0.5 V_{dc}	V_{dc}
Fig 5(b)	Inverter mode (a)	grid, L_2, D_1, S_5, and L_1	grid, L_2, ($S_6(D_{S6})$, $S_7+S_8(D_{S7})$, S_5) and L_1	0.5 V_{dc}	0
Fig 5(c)	Inverter mode (a)	grid, L_1, S_3, dc side, S2, S6 and L_2	grid, L_1, S_3, dc side, S2, S6 and L_2	0.5 V_{dc}	-V_{dc}
Fig 5(d)	Inverter mode (a)	grid, L_2, D_1, S_3 and L_1	grid, L_1, ($S_5(D_{S5})$, $S_8+S_7(D_{S7})$, S_6) and L_2	0.5 V_{dc}	0
Fig 6(a)	Rectifier mode (a)	gird, L_1, D_2, S_6 and L_2	grid, L_1, $S_7(D_{S7})$, D_{S2}, dc side, $S_4(D_{S4})$ and L_2	0.5 V_{dc}	0
Fig 6(b)	Rectifier mode (b)	gird, L_1, D_2, D_{S2}, dc side, $S_4(D_{S4})$ and L_2	grid, L_1, $S_5(D_{S5})$, $S_8+S_7(D_{S7})$, S_6 and L_2	0.5 V_{dc}	V_{dc}
Fig 6(c)	Rectifier mode (c)	gird, L_2, D_1, S_5 and L_1	grid, L_2, ($S_8(D_{S8})$, D_{S1}, dc side, $S_3(D_{S3})$ and L_1	0.5 V_{dc}	0
Fig 6(d)	Rectifier mode (d)	gird, L_2, D_1, D_{S1}, dc side, $S_3(D_{S3})$ and L_1	grid, L_2, $S_6(D_{S6})$, $S_7+S_8(D_{S8})$, S_5 and L_1	0.5 V_{dc}	-V_{dc}

TABLE 2. Power components of standard and synchronous H6 demonstrator circuits.

Components	Model number	Rated voltage (V)	Rated current (A)
SiC MOSFET	C3M0120090D	900	23
SiC Schottky diode	CVFD20065A	650	26
Inductor	500μ H	-	24
Inductor type	MPP 0055617A2	-	-
Capacitor AC	4.7 μF	250	-
Capacitor DC	3760 μF	450	-

By comparing the inductor's current to the grid reference current *Iref*, a second control loop can ensure that the inductor is accurately tracking *Iref*.

III. ANALYSIS AND DESIGN CONSIDERATION

A. DEVICE SELECTION

A 380 Vdc is used for the DC side of the H6 transformer-less inverter topologies, and 220 Vac and 50 Hz are assumed for the grid side. The table below, Table 2, provides a list of the switching and passive components that were chosen for a maximum power rating of 5 kW at a switching frequency, Fsw, of 20 kHz. In both the standard H6 and the proposed synchronous H6, the SiC MOSFETs used for the S1-S6 and S1-S8 switches were the same.

B. SEMICONDUCTORS LOSS [35], [36]

Conduction loss of the SiC MOSFETs (P_{cm}), MOSFET body-diodes, (P_{cantid}) and diodes (P_{cd}) are given as:

$$Pcm = R_{dson\_s}I^2_{rms\_s} \quad (1)$$

$$Pcd = V_{fsd}I_{av\_d} + R_{dson\_d}I^2_{rms\_d} \quad (2)$$

$$Pc_{anti}d = V_{fsm}I_{av\_md} + R_{dson\_d}I^2_{rms\_md} \quad (3)$$

respectively, where R_{dson_x} is on resistance of the given component, while I_{rmx_x} is its rms current, V_{fsx} is the given diode component forward voltage drop and I_{av_x} is its average current. Switching loss of SiC MOSFETs (P_{swonm}, P_{swoffm}) and diodes (P_{swond}, P_{swoffd}) are given as:

$$Psw_{on}m = \left(V_{pkm\_on}I_{pkm\_on}\frac{Tr}{2} + Q_{rr}V_{pkm\_on}\right)F_{sw} \quad (4)$$

$$Psw_{off}m = \left(V_{pkm\_off}I_{pkm\_off}\frac{Tf}{2}\right)F_{sw} \quad (5)$$

$$Psw_{on}d = \frac{1}{4}\left(V_{pkd\_off}Q_{rr}\right)F_{sw} \quad (6)$$

where, Tr & Tf are rise and fall times of the MOSFETs during switching, Q_{rr} is a reverse recovery charge of the given diode, Vf and If are diode forward voltage and current, whereas, F_{sw} is the carrier switching frequency. Finally, MOSFET gate charge losses in (7) are given in terms of high & low side electric charge, Q, and capacitance, C, values as provided in the MOSFET datasheet:

$$Pg = ((Q_{g-h}Q_{g-l})V_{gs}F_{sw}) + ((C_{g-h}C_{g-l})V^2_{gs}F_{sw}) \quad (7)$$

Using PSIM simulation, representative values of peak, average and rms voltages and currents were measured for each component at four different time samples of each half cycle, and these were applied in (1-7) to calculate the circuit loss breakdown for different power level.

(a)

(b)

(c)

(d)
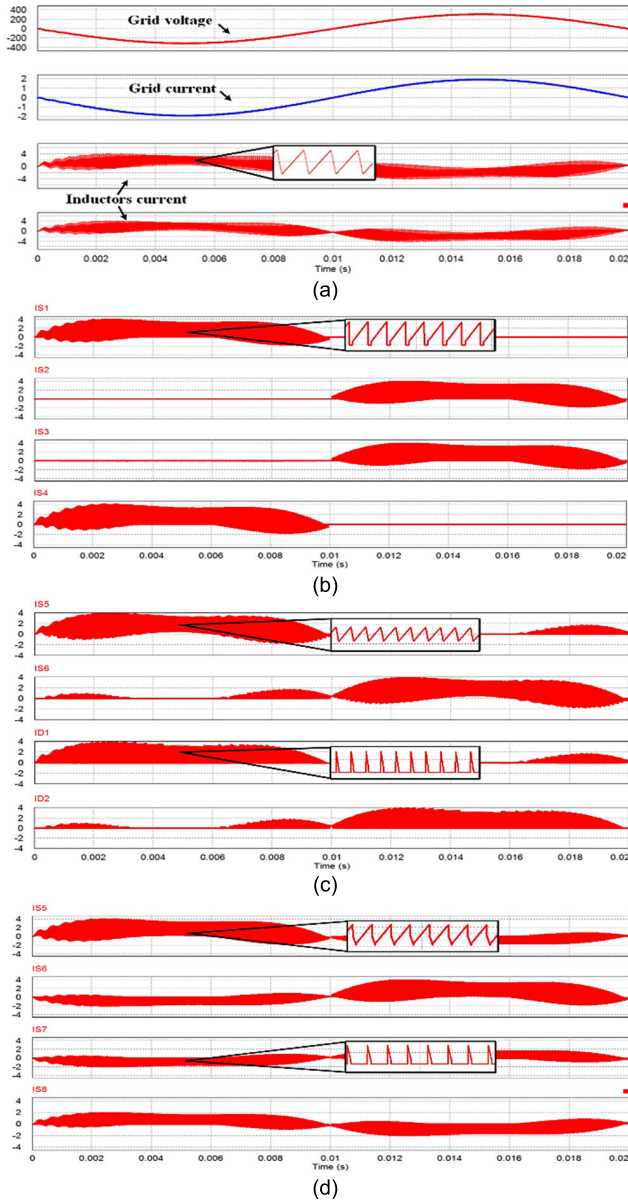
FIGURE 8. Light-load (300W) performance for inversion mode (a) Grid voltage & current and inductors current of synchronous H6, (b) SiC MOSFETs S1-S4 of synchronous H6, (c) Diodes D1 & D2 and SiC MOSFETs S5 & S6 waveforms of standard H6, (d) SiC MOSFETs S5-S8 waveforms of synchronous H6.
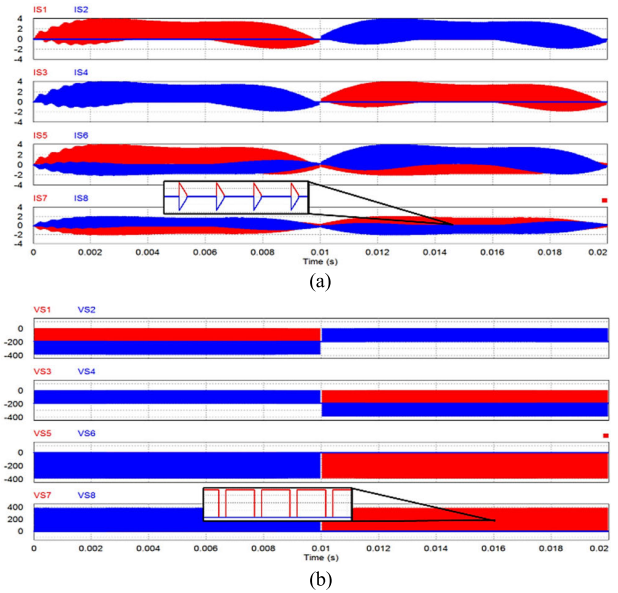
C. LCL FILTER LOSS [37], [38]

The DC link and AC capacitor were chosen based on the following:

$$C_{dc} = \frac{I_{load}}{8\pi F V_{ripple}} \tag{8}$$

$$C_{ac} = \frac{I_{load}}{2F_{sw} V_{ripple}} \tag{9}$$

where I_{load} represents the current load and V_{ripple} represents the needed ripple voltage.

(a)

(b)

FIGURE 9. Switches operation of synchronous H6 inverter (a) current waveforms and (b) voltage waveforms operation at 300W.

Copper and core losses, (P_{copper}, P_{core}) in the filter inductors are calculated according to:

$$\mathrm{P}copper = I_{rms}^2 R_{wire} \tag{10}$$

$$\mathrm{P}core = \frac{\mathrm{PL\ Ae\ Le}}{1000} \tag{11}$$

$$\mathrm{PL} = 31.32\ \Delta\ \beta^{1.585} 20^{1.37} \tag{12}$$

where Ae is the cross-section area of the core, Le its path length and PL is core loss density as a function of AC flux $\Delta\beta$, frequency (kHz) and the given material constants. The equivalent series resistance (ESR) loss of the capacitor is given as

$$Pca = I_{rms}^2\ ER \tag{13}$$

IV. SIMULATION RESULTS
A. CIRCUIT OPERATION

Figure 8 (a) shows simulated results of the proposed synchronous H6 waveforms in inverter mode, and confirms that a balanced grid output voltage and current are achieved. Representative waveforms of SiC MOSFETs S1-S4 at light-load (10%) are presented in Figure 8 (b) which are the same as for a standard H6. The waveforms of diodes D1 & D2 and SiC MOSFETs S5 & S6 of an equivalent standard H6 are given in Figure 8 (c) for comparison with the synchronous H6 SiC MOSFETs S5-S8 in Figure 8 (d). As shown, the inductor current is divided into two paths during the dead time (through S8 & S5 and through S6 & S7), and this provides significant loss reduction. It is apparent from the D1 and D2 waveforms of the standard H6 that their current are continuous for light-load condition compared to the high-load due to the effect introduced by the inductor (IL1 & IL2).
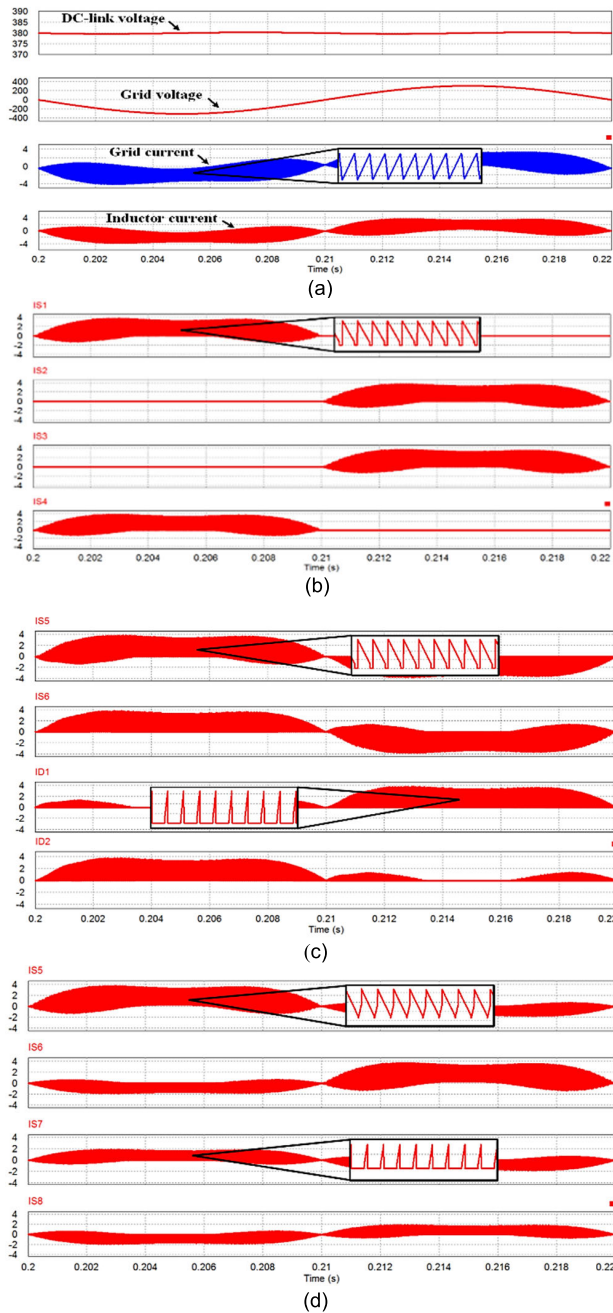
FIGURE 10. Light-load (300W) performance for rectification mode (a) Grid voltage & current and inductors current of synchronous H6, (b) SiC MOSFETs S1-S4 of synchronous H6, (c) Diodes D1 & D2 and SiC MOSFETs S5 & S6 waveforms of standard H6, (d) SiC MOSFETs S5-S8 waveforms of synchronous H6.

The operational current waveforms of switches (S1-S8) of the proposed synchronous H6 in inversion mode are presented in Figure 9 (a). It is observed that S5-S8 are operated during full cyle compared to S1-S4 where the current was almost double its value in S1-S4. The voltage waveforms of the same as shown in Figure 9 (b). A positive correlation with predictions was found between S5 & 6 and S7 & S8 in terms of blocking the DC voltage.
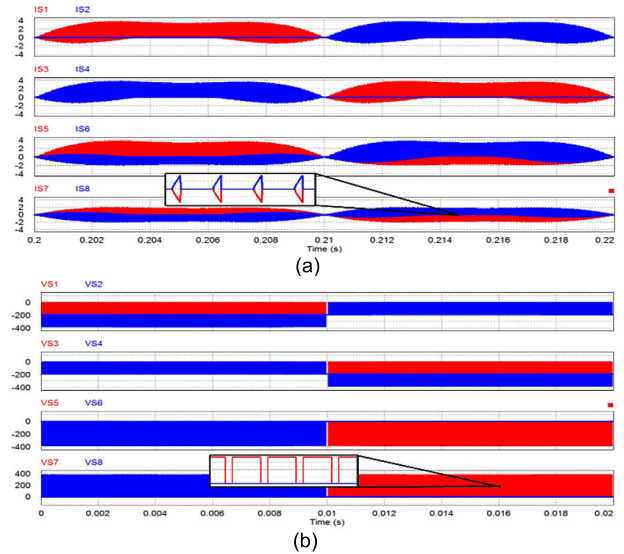

FIGURE 11. Switches operation of synchronous H6 rectifier (a) current waveforms and (b) voltage waveforms at 300W.

Figure 10 (a) displays simulated results of the proposed synchronous H6 waveforms in rectifier mode, and again confirms that a sinusoidal current in phase with the voltage, and balanced grid output voltage and current is achieved. Representative waveforms of SiC MOSFETs S1-S4 at light- load (10%) are presented in Figure 10 (b) which are the same as for a standard H6. The waveforms of diodes D1& D2 and SiC MOSFETs S5 & S6 of an equivalent standard H6 are given in Fig 10 (c) for comparison with the synchronous H6 SiC MOSFETs S5 – S8 in Figure 10 (d). As shown, the inductor current is divided into two paths during the off time (through S8 & S5 and through S6 & S7), and this provides significant loss reduction. A continuous current flows through D1 and D2 of the standard H6 for a light-load compared to high load due to the inductor impact (IL1 & IL2).

The operational current waveforms of switches (S1-S8) of the synchronous H6 in rectifier mode are presented in Figure 11(a). It is similar to the inverter mode, where S5-S8 are operated during full cycle and have a current value of almost double the current through S1-S4. The voltage waveforms of the same switches (S1-S8) are shown in Figure 11(b).
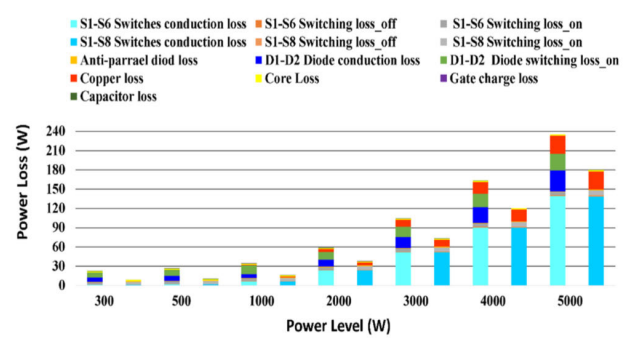
The control strategy of the proposed synchronous H6 is set to guarantee a fast response following the sudden change of the load condition. Figure12 (a) shows the transient response of the designed controller operated at light-load conditions i.e. 300W to 500W and vice-versa for grid current & voltage as well as DC voltage and current. Likewise, when the load condition is varied up to 1000W, the control tracks the desired value and guarantees the stability of the design topology. In terms of high load operation, Figure12 (c) shows the transient and dynamic response of the grid current & voltage and DC output voltage and current ranging from 4 kW to 5 kW.
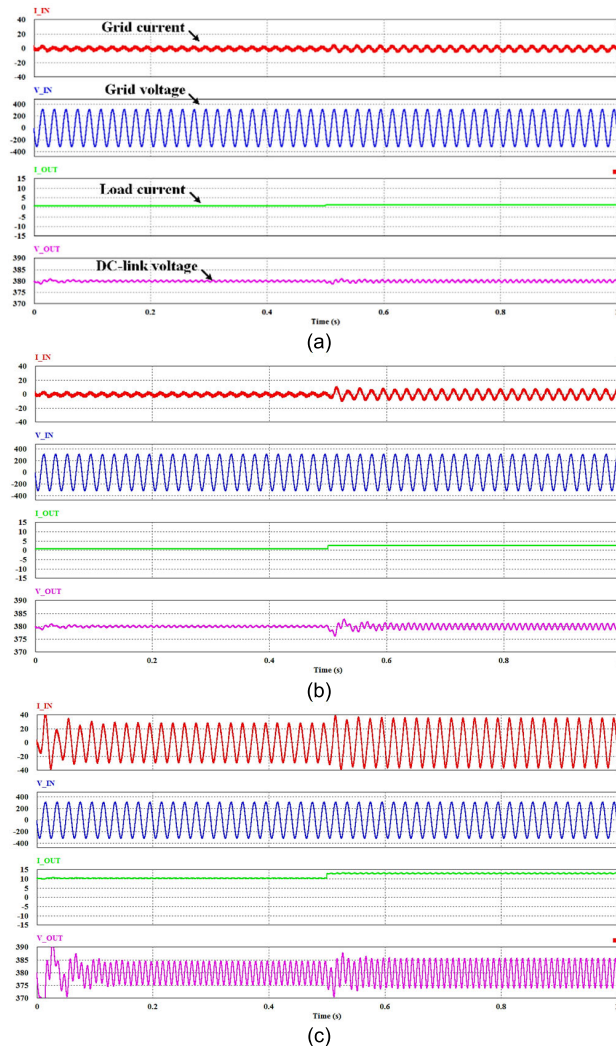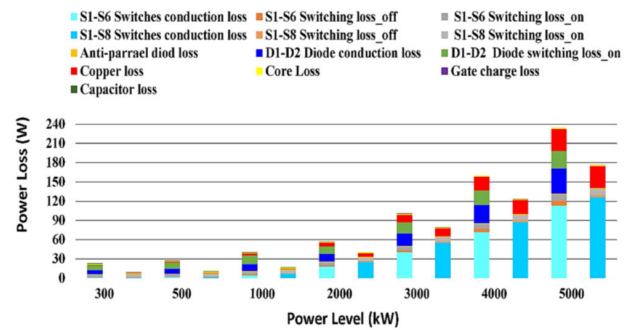
FIGURE 12. Transient respond of input and out current & voltage of synchronous H6 at rectifier mode under different load conditions (a) 300W - 500W, (b) 300W - 1000W and from 4000W -5000W.

FIGURE 13. Power loss breakdown at inverter mode of Synchronous vs. Standard H6 topologies.

FIGURE 14. Power loss breakdown at rectifier mode of Synchronous vs. Standard H6 topologies.

B. LOSS BREAKDOWN AND EFFICIENCY COMPARISON

Analysis of the loss breakdown in Figure 13(a) shows a significant contribution in SiC MOSFETS and diode switching ON losses and related conduction by the diode at light-load for the standard H6. As shown in Figure13 (b), these dominant losses are reduced in the proposed synchronous H6 to 9% and 86% for SiC MOSFETs and diode switching ON losses respectively whereas, the diodes conduction loss is decreased by 96.4% when replaced by switches (S7 & S8). It was found that such an approach can achieve high efficiency at 98.5% for both inverter and rectifier modes at light-load where a comparative efficiency obtained from the two analysed H6 topologies is presented in Figure 15. The most striking observation is the improved light-load efficiency provided by the proposed synchronous topology, while the efficiency of both standard and synchronous H6 tends to decrease when the operational power is increased towards its design limit.

Similarly, the analysis of the loss breakdown in Figure 14 shows a significant contribution in SiC MOSFETS and diode switching on losses and related conduction by the diode at light-load for the standard H6. The operational principle of the rectifier in both designs enabled the MOSFETs body diode for supplying the DC load demand, which result in addition loss in this stage of conversion. In Figure 14, these dominant losses are reduced in the proposed synchronous H6 to 8% and 98% for SiC MOSFETs and diode switching on losses respectively, whereas, the diode conduction loss is decreased by 96.4% when replaced by switches (S7 & S8). The results achieved surpass the earlier work of the standard H6 topology in terms of light-load efficiency at 98.5% utilising synchronous H6 topology.

A comparison of the efficiency for inverter and rectifier modes obtained for the two H6 topologies are presented in Figure 15. The more surprising correlation is with the improved light-load efficiency provided by the proposed synchronous topology, while the efficiency of both standard and synchronous H6 tends to decrease when the operational power is increased towards its design limit. It is perhaps worth noting that the contribution of the SiC MOSFETs body diode could result in an additional power loss in the case of rectifier mode operation as the relevant current path is enabled during this model's operation, as was previously stated.
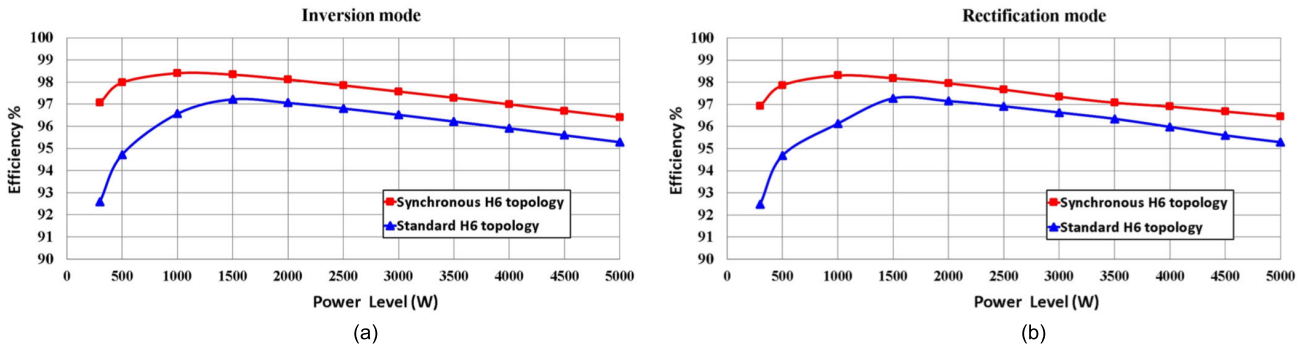
FIGURE 15. Efficiency comparison of H6 at; (a) inverter mode and (b) rectifier mode.
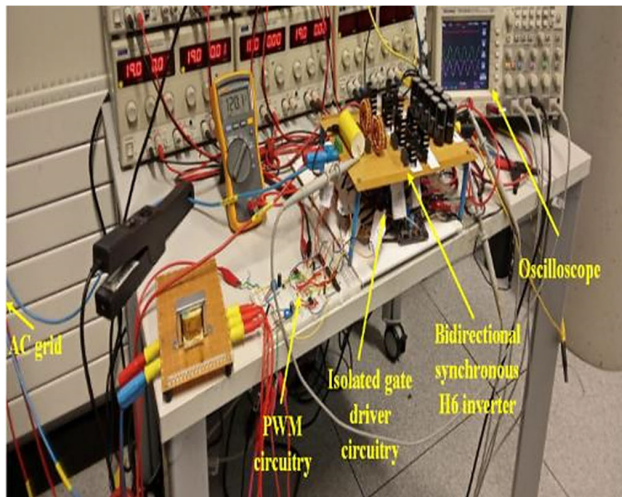

FIGURE 16. Photograph of a hardware prototype of the 1-kW synchronous H6 inverter in a test-bed setup.

FIGURE 17. Synchronous H6 at inverter and rectifier modes (a) Pluses of the PWM waveforms and (b) pluses of a zoomed-in PWM waveform.

V. EXPERIMENTAL RESULTS

To validate modelled results, a 1 kW demonstration system is used as the experimental basis for this study, with all components chosen to fit the specification of the resized 1 kW model. Figure 16 also depicts a bidirectional prototype with a rated power output of 1-kW, which is based on the synchronous H6 type design. The findings of the tests that were carried out are discussed in more detail below which is composed of two parts: inverter mode and rectifier mode. 120 Vdc is used to evaluate H6 transformer-less inverter topologies, and 63 Vac and 50 Hz are given for the AC side. Table 3 shows the components selected for a maximum power rating of 1 kW at a switching frequency of 20 kHz. The same SiC MOSFETs were utilized for S1 – S6 in the standard H6 and for S1– S8 in the proposed synchronous H6.

The implementation of control circuitry to generate gate signals that required to drive the utilized switch is further discussed. It is shown that regardless of whether the bidirectional synchronous H6 inverter is an inverter or a rectifier, its switching pattern is the same. This means that the same PWM
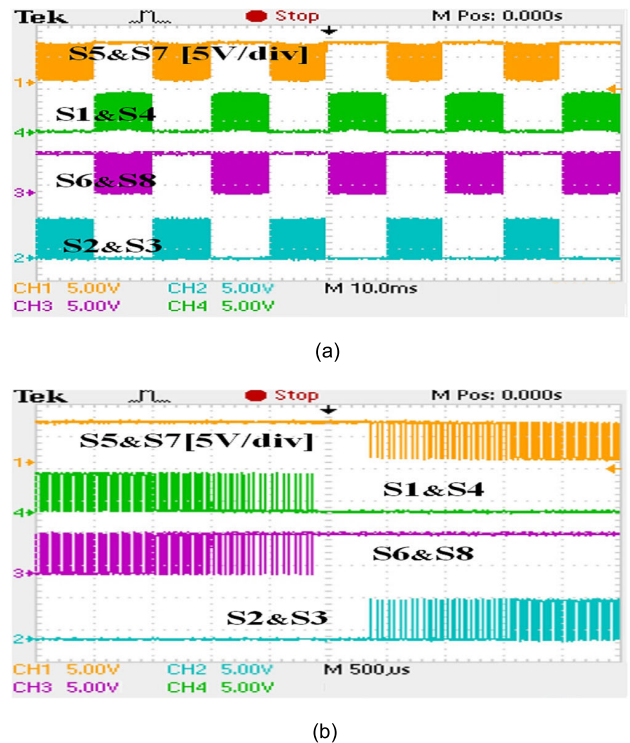
modulation control is used for both inversion and rectification modes, as seen in Figure 17.

In order to maximize the performance of such technology (SiC MOSFETS) used in the bidirectional synchronous H6, it is advised that the SiC MOSFET be operated between (+15V and -4V) which required a negative gate signal in comparison to other switches such as Si MOSFET [39]. This is due to the characteristic of fast switching of SiC MOSFET which required an efficient turn off. In addition, this is required since extending the scope beyond the specified range might result in shoot-through, which would increase the switching loss. Because of this, circuitry was developed
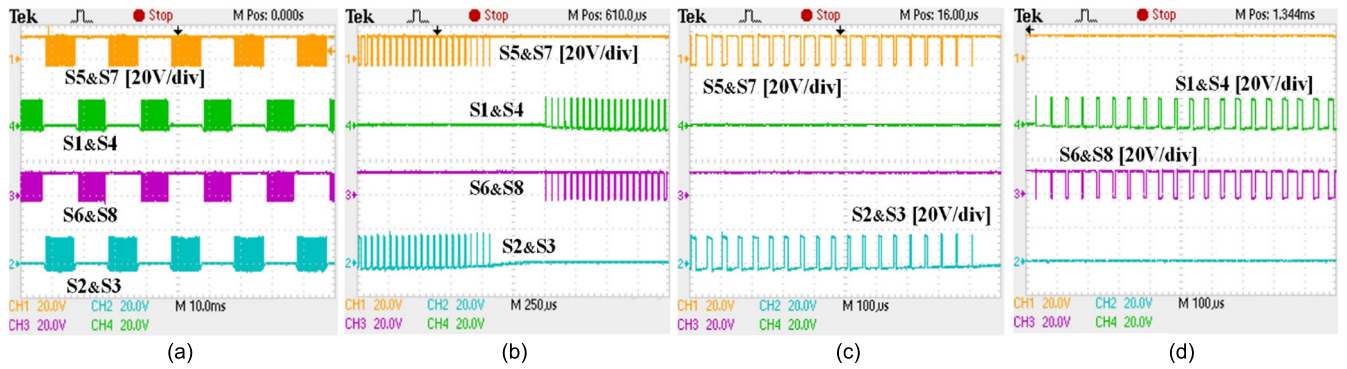
FIGURE 18. The output pluses of gate drivers for SiC MOSFETs (a) S1-S8 switches, (b) zoomed-in S1-S8 switches and (c) S5 & S7 and (d) S1 & S4 switches expanded.
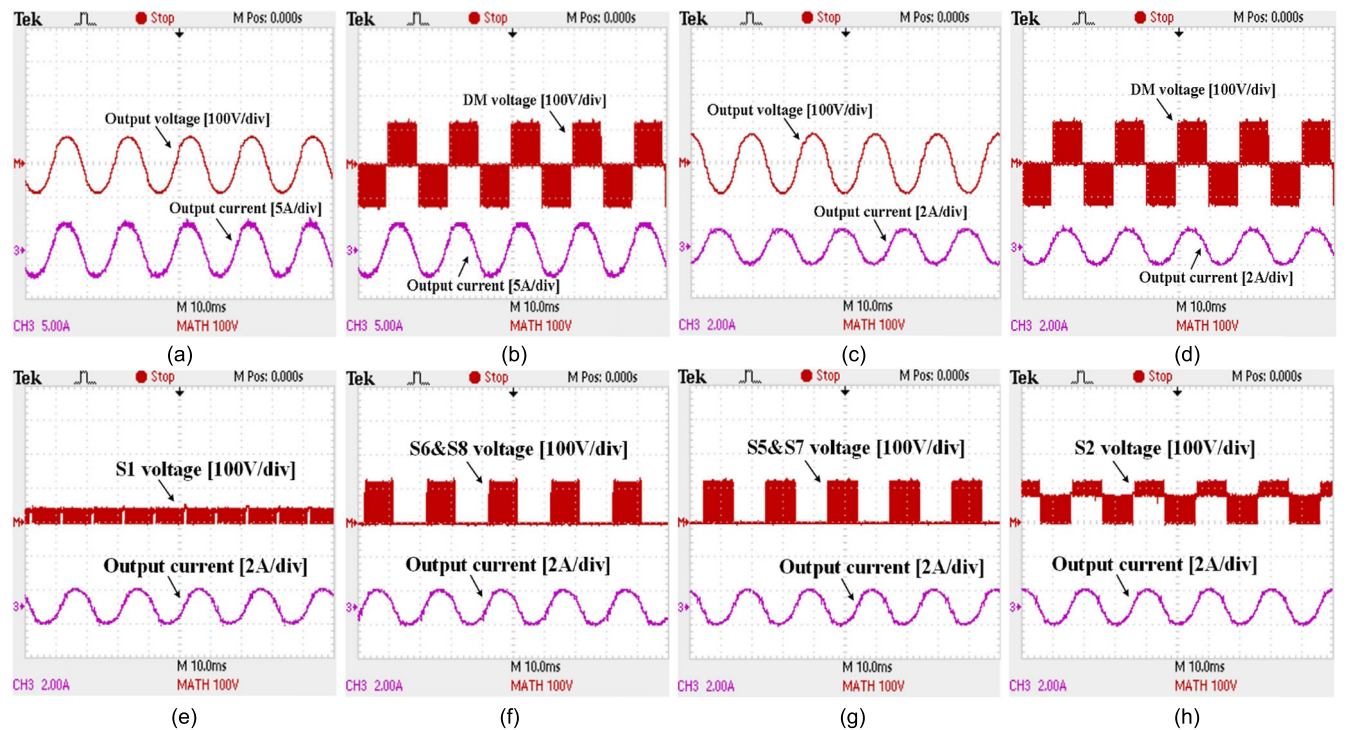
FIGURE 19. Measurement waveforms of synchronous H6 at inverter mode (a) output voltage and current at full load (200W), (d) DM voltage at full load (200W), (c) output voltage and current at light-load (50W), (d) DM voltage at light-load (50W), (e) S1 switching voltage, (f) S6&S8 switching voltage and (g) S5&S7 switching voltage (h) S1 and S2 switching voltage.

to provide the required voltage range for efficient operation, as can be seen in Figure 18.

The output voltage and ac current of bidirectional synchronous H6 operating at inverter mode under 20% load of (200W) and light-load of (50W) are shown in Figure 19 (a) and (c). These values are in phase with the grid frequency of 50Hz. The inverter mode waveforms have a power factor (PF) of 1, and the bidirectional synchronous H6 inverter has a DC-link voltage of 120 Vdc. The inverter mode has a relatively low total harmonic distortion (THD) for the grid current, which indicates high performance for the grid current under light-load condition (50W). It is important to note that the THD of current decreases when the bidirectional

synchronous H6 operates at a power level greater than 100W, which results in a return to improved efficiency.

Figure 19 (b) and (d) show the differential mode (DM) voltage as well as the ac current when the prototype is operating in inverter mode at 200W and 50W respectively. Typically, +1, 0 and -1 three level voltages illustrate its DM voltage advantages, while constant dc voltage with minimal ac ripple confirms the feature of eliminating the CM and leakage current that exists in H6 topologies including the proposed synchronous topology.

Figure 19 (e) is an illustration of the switching voltage waveform at 50W that exists during the conduction period of the high side switch (S1), and it is identical to the switching

(a)   (b)   (c)   (d)
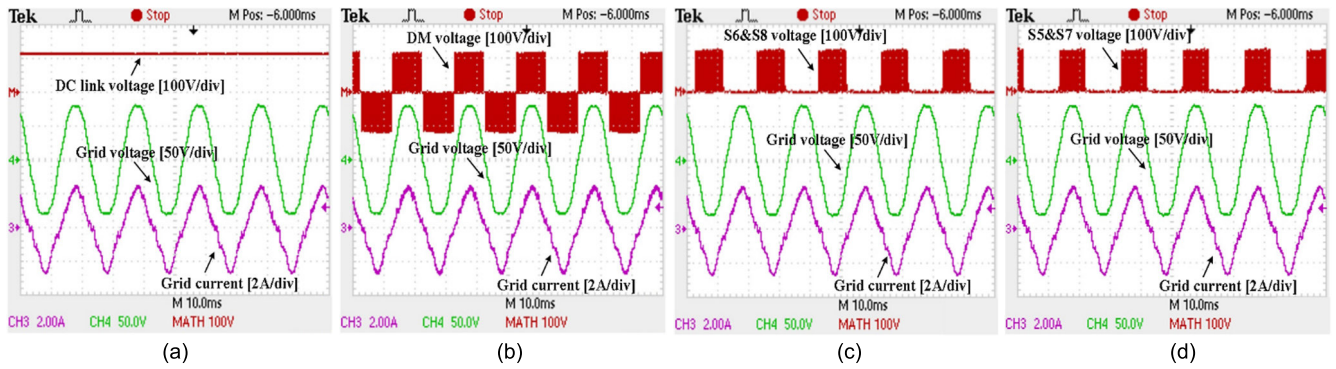
FIGURE 20. Measured and simulated results of the efficiency of 1-kW system for synchronous and standard H6 under 20kHz operating frequency at (a) inverter mode and (b) rectifier mode.

TABLE 3. Power components of standard and synchronous H6 demonstrator circuits.

Components	Model number	Rated voltage (V)	Rated current (A)
SiC MOSFET	C3M0280090D	900	11.5
SiC Schottky diode	C6D10065A	650	10
Inductor (MPP core)	500µ H	200	10
Capacitor AC	4.7 µF	160	12
Capacitor DC	3760 µF	220	13
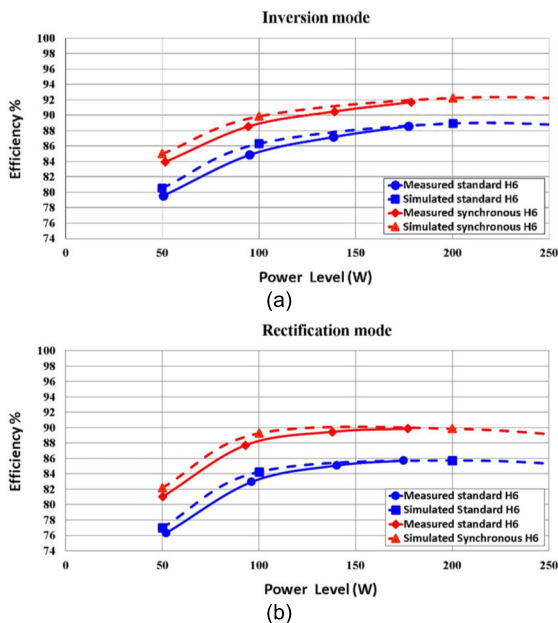
FIGURE 21. Measurement waveforms of synchronous H6 at inverter mode (a) DC-link voltage with grid voltage and current, (b) DM voltage, (c) S6&S8 switching voltage, (d) S5&S7 switching voltage.

voltage waveform that exists for the other high side switch (S3) that operates during the negative grid cycle. The switching voltage is depicted in Figure 19 (f) and (g) when the meddle switches S5&S7 and S6&S8 are conducting respectively. Both S5&S7 and S6&S8 perform operations that are mirror images of one another and are therefore symmetrical. Figure 19 (h) depicts the switching voltage applied to the low

side switches (S2) during conducting, with the same voltage being applied to the other low side switch (S4) throughout the positive grid half cycle.

Figure 20 (a) shows the input voltage and ac current of a bidirectional synchronous H6 operating in rectifier mode at light-load (50W). These measurements are in phase with the 50 Hz grid frequency, indicating that the ac grid current and grid voltage are synchronized. The rectifier mode waveforms of voltage and current are in phase, and the output synchronous H6 inverter has a DC link voltage of roughly 120 Vdc. This demonstrates that the proposed synchronous H6 inverter boosted the grid voltage by 66%, as indicated by the modulation index. The rectifier mode has a higher THD for the grid current, indicating lower performance for the grid current under light-load conditions (50W) than the inverter mode. However, this could be overcome by designing a suitable AC filter or by modifying the PWM to enhance the performance of grid current during rectifier mode.

When the synchronous H6 operates in rectifier mode, the ac current and DM voltage are shown in Figure 20(b) and (d). Standard DM voltages of +1, 0 and -1 levels demonstrate its merits, while a relatively steady dc voltage with negligible ac ripple demonstrates the feature of reducing CM and leakage current in a way that corresponds to that of operation in invert mode.

The switching voltages in Figure 20 (d) and (e) indicate when middle switches S5&S7 and S6&S8 are conducting, respectively. Furthermore, S5&S7 and S6&S8 are symmetrical, as their operations are similar. During S1's conduction interval, the switching voltage waveform is the same as S3, which operates during the negative grid cycle and has the same switching voltage for inverter mode but corresponds to the DC-link voltage. In addition, during inverter mode, the DC-link voltage corresponds with the conduction period of the switching voltage waveform for both low side switch (S2) and high side switch (S4).

Finally, Figure 21 depicts the efficiency curves of both inverter and rectifier modes for the standard and proposed synchronous H6 inverter. In both inverter and rectifier modes, the proposed synchronous H6's efficiency is up to 3.8%

and 3.9% respectively higher than that of the standard H6 at 20% load. It was determined through simulation that the 1 kW synchronous H6 had an overall maximum efficiency of 92.7% when operating in the inversion mode and 89.8% when operating in the rectification mode. However, at 20% load the 1 kW synchronous H6's simulated efficiency is up to 2% higher than the measured efficiency reported. Since controller and snubber circuitry losses were accounted for in the simulation, this discrepancy between simulated and experimental results may be due to accuracy of the measurement equipment. Also, external disturbances of equipment, as well as component material deterioration, contribute to variations between experimental and simulation findings. Compared to the synchronous H6 inverter mode, the rectifier mode results in higher switching losses due to the high frequency switching of two switches and the use of MOSFETs body-diodes for corresponding current paths. Such is the cost of giving the synchronous H6 a rectifier mode like the regular H6 in consideration for bidirectional power capability. Compared to synchronous H6 a rectifier mode like the regular H6 in consideration for bidirectional power capability. Compared to the efficiency of the inverter mode, the efficiency given by the synchronous H6 at the rectifier is lower. Despite the fact that the efficiency of the small-scale porotype demonstrator is higher than that of the standard H6 topology, it is predicted that the efficiency of the inverter and rectifier mode of the 5-kW systems would improve. As a result of a smaller R_{dson} value of the semiconductor devices in the 5-kW system compared to the 1-kW system, the conduction loss at light-load condition (20%) will be reduced.

VI. CONCLUSION

A bidirectional inverter's energy efficiency during light-load conditions may be increased for the purpose of improving the total energy efficiency of a PV-powered DC distribution system that is employed in a residential application. An optimal configuration of an existing bidirectional inverter is investigated and optimized to significantly enhance light-load efficiency. By comparison, the proposed 5-kW synchronous H6 transformer-less topology has been reported to achieve a predicted improvement in efficiency of up to 98.3%, while a standard H6 can achieve an efficiency of 92.5% for loads under 20%. The rectifier mode also saw marked improvement, with up to 98.1% provided compared to 92.4% under light operational load levels. As a result of the relative contribution of diode conduction and switching on loss under different load conditions, this improvement has been achieved. The results of the experiments demonstrate that the proposed bidirectional synchronous H6 inverter is capable of achieving the anticipated level of improvement under light-load conditions.

ACKNOWLEDGMENT

REFERENCES

[1] D. Fregosi, S. Ravula, D. Brhlik, J. Saussele, S. Frank, E. Bonnema, J. Scheib, and E. Wilson, "A comparative study of DC and AC microgrids in commercial buildings across different climates and operating profiles," in *Proc. IEEE 1st Int. Conf. DC Microgrids (ICDCM)*, Jun. 2015, pp. 159–164.

[2] F. L. Franco, A. Morandi, P. Raboni, and G. Grandi, "Efficiency comparison of DC and AC coupling solutions for large-scale PV+BESS power plants," *Energies*, vol. 14, no. 16, p. 4823, Aug. 2021.

[3] A. Pratt, P. Kumar, and T. V. Aldridge, "Evaluation of 400 V DC distribution in Telco and data centers to improve energy efficiency," in *Proc. 29th Int. Telecommun. Energy Conf.*, Sep. 2007, pp. 32–39.

[4] M. Alshammari and M. Duffy, "Feasibility analysis of a DC distribution system for a 6 kW photovoltaic installation in Ireland," *Energies*, vol. 14, no. 19, p. 6265, Oct. 2021.

[5] M. Alshammari and M. Duffy, "Comparative analysis between AC and DC distribution systems in a photovoltaic system: A case study of a school in Ireland," in *Proc. Int. Exhib. Conf. Power Electron., Intell. Motion, Renew. Energy Energy Manage.*, May 2019, pp. 7–9.

[6] M. C. Kisacikoglu, M. Kesler, and L. M. Tolbert, "Single-phase on-board bidirectional PEV charger for V2G reactive power operation," *IEEE Trans. Smart Grid*, vol. 6, no. 2, pp. 767–775, Mar. 2015.

[7] J. Yuan, L. Dorn-Gomba, A. D. Callegaro, J. Reimers, and A. Emadi, "A review of bidirectional on-board chargers for electric vehicles," *IEEE Access*, vol. 9, pp. 51501–51518, 2021.

[8] S. Taghizadeh, M. J. Hossain, N. Poursafar, J. Lu, and G. Konstantinou, "A multifunctional single-phase EV on-board charger with a new V2V charging assistance capability," *IEEE Access*, vol. 8, pp. 116812–116823, 2020.

[9] M. Yilmaz and P. T. Krein, "Review of battery charger topologies, charging power levels, and infrastructure for plug-in electric and hybrid vehicles," *IEEE Trans. Power Electron.*, vol. 28, no. 5, pp. 2151–2169, May 2013.

[10] K. Kroics, O. Husev, K. Tytelmaier, J. Zakis, and O. Veligorskyi, "An overview of bidirectional AC–DC grid connected converter topologies for low voltage battery integration," *Int. J. Power Electron. Drive Syst. (IJPEDS)*, vol. 9, no. 3, p. 1223, Sep. 2018.

[11] B. Gu, J. Dominic, B. Chen, and J. S. Lai, "A high-efficiency single-phase bidirectional AC–DC converter with minimized common mode voltages for battery energy storage systems," in *Proc. IEEE Energy Convers. Congr. Expo.*, Sep. 2013, pp. 5145–5149.

[12] H. Qian, J.-S. Lai, and W. Yu, "Novel bidirectional AC–DC MOSFET converter for energy storage system applications," in *Proc. IEEE Energy Convers. Congr. Expo.*, Sep. 2011, pp. 3466–3471.

[13] M. Nassary, M. Orabi, M. Ghoneima, and M. K. El-Nemr, "Single-phase isolated bidirectional AC–DC battery charger for electric vehicle—Review," in *Proc. Int. Conf. Innov. Trends Comput. Eng. (ITCE)*, Feb. 2019, pp. 581–586.

[14] S. Dharmasena, T. O. Olowu, and A. I. Sarwat, "Bidirectional AC/DC converter topologies?: A review," in *Proc. SoutheastCon*, 2019, pp. 1–5.

[15] B. Koushki, A. Safaee, P. Jain, and A. Bakhshai, "A bi-directional single-stage isolated AC–DC converter for EV charging and V2G," in *Proc. IEEE Electr. Power Energy Conf. (EPEC)*, Oct. 2015, pp. 36–44.

[16] H. Chen, X. Wang, and A. Khaligh, "A single stage integrated bidirectional AC/DC and DC/DC converter for plug-in hybrid electric vehicles," in *Proc. IEEE Vehicle Power Propuls. Conf.*, vol. 2, Sep. 2011, pp. 1–6.

[17] M. Islam, S. Mekhilef, and M. Hasan, "Single phase transformerless inverter topologies for grid-tied photovoltaic system: A review," *Renew. Sustain. Energy Rev.*, vol. 45, pp. 69–86, May 2015.

[18] F. Chen, R. Burgos, and D. Boroyevich, "A high-efficiency interleaved single-phase AC–DC converter with common-mode voltage regulation for 380 V DC microgrids," in *Proc. IEEE Energy Convers. Congr. Expo. (ECCE)*, Oct. 2017, pp. 4128–4135.

[19] W. Li, Y. Gu, H. Luo, W. Cui, X. He, and C. Xia, "Topology review and derivation methodology of single-phase transformerless photovoltaic inverters for leakage current suppression," *IEEE Trans. Ind. Electron.*, vol. 62, no. 7, pp. 4537–4551, Jul. 2015.

[20] A. Khan, L. Ben-Brahim, A. Gastli, and M. Benammar, "Review and simulation of leakage current in transformerless microinverters for PV applications," *Renew. Sustain. Energy Rev.*, vol. 74, pp. 1240–1256, Jul. 2017.

[21] T. Dragičević, X. Lu, J. C. Vasquez, and J. M. Guerrero, "DC microgrids—Part II: A review of power architectures, applications, and standardization issues," *IEEE Trans. Power Electron.*, vol. 31, no. 5, pp. 3528–3549, May 2016.

[22] D. Dong, F. Luo, D. Boroyevich, and P. Mattavelli, "Leakage current reduction in a single-phase bidirectional AC–DC full-bridge inverter," *IEEE Trans. Power Electron.*, vol. 27, no. 10, pp. 4281–4291, Oct. 2012.

[23] M. N. H. Khan, M. Forouzesh, Y. P. Siwakoti, L. Li, T. Kerekes, and F. Blaabjerg, "Transformerless inverter topologies for single-phase photovoltaic systems: A comparative review," *IEEE J. Emerg. Sel. Topics Power Electron.*, vol. 8, no. 1, pp. 805–835, Mar. 2020.

[24] C. Liu, Y. Wang, J. Cui, Y. Zhi, M. Liu, and G. Cai, "Transformerless photovoltaic inverter based on interleaving high-frequency legs having bidirectional capability," *IEEE Trans. Power Electron.*, vol. 31, no. 2, pp. 1131–1142, Feb. 2016.

[25] T.-F. Wu, K.-H. Sun, C.-L. Kuo, and C.-H. Chang, "Predictive current controlled 5-kW single-phase bidirectional inverter with wide inductance variation for DC-microgrid applications," *IEEE Trans. Power Electron.*, vol. 25, no. 12, pp. 3076–3084, Dec. 2010.

[26] F. Chen, R. Burgos, and D. Boroyevich, "Efficiency comparison of a single-phase grid-interface bidirectional AC/DC converter for DC distribution systems," in *Proc. IEEE Energy Convers. Congr. Expo.*, Sep. 2015, pp. 6261–6268.

[27] S. H. Lee, K.-T. Kim, J.-M. Kwon, and B.-H. Kwon, "Single-phase transformerless bi-directional inverter with high efficiency and low leakage current," *IET Power Electron.*, vol. 7, no. 2, pp. 451–458, Feb. 2013.

[28] F. Chen, R. Burgos, D. Boroyevich, and X. Zhang, "Low-frequency common-mode voltage control for systems interconnected with power converters," *IEEE Trans. Ind. Electron.*, vol. 64, no. 1, pp. 873–882, Jan. 2017.

[29] F. Chen, R. Burgos, and D. Boroyevich, "A bidirectional high-efficiency transformerless converter with common-mode decoupling for the interconnection of AC and DC grids," *IEEE Trans. Power Electron.*, vol. 34, no. 2, pp. 1317–1333, Feb. 2019.

[30] B. Ji, J. Wang, and J. Zhao, "High-efficiency single-phase transformerless PV H6 inverter with hybrid modulation method," *IEEE Trans. Ind. Electron.*, vol. 60, no. 5, pp. 2104–2115, May 2013.

[31] J. Wang, F. Luo, Z. Ji, Y. Sun, B. Ji, W. Gu, and J. Zhao, "An improved hybrid modulation method for the single-phase H6 inverter with reactive power compensation," *IEEE Trans. Power Electron.*, vol. 33, no. 9, pp. 7674–7683, Sep. 2018.

[32] J. Wang, S. Gao, Y. Sun, Z. Ji, L. Cheng, L. Li, W. Gu, and J. Zhao, "Single phase bidirectional H6 rectifier/inverter," *IEEE Trans. Power Electron.*, vol. 34, no. 11, pp. 10710–10719, Nov. 2019.

[33] M. Alshammari and M. Duffy, "Review of single-phase bidirectional inverter topologies for renewable energy systems with DC distribution," *Energies*, vol. 15, no. 18, p. 6836, Sep. 2022.

[34] M. Alshammari and M. Duffy, "A novel synchronous H6 for improving light load efficiency of bidirectional inverters in a DC distribution system," in *Proc. IEEE Appl. Power Electron. Conf. Expo. (APEC)*, Jun. 2021, pp. 1666–1673.

[35] D. Graovac, M. Purschel, and K. Andreas, "MOSFET power losses calculation using the data-sheet parameters," *Infineon Appl.*, vol. 1, pp. 1–23, Jul. 2006.

[36] *Calculation of Power Loss Synchronous Converter*, Rohm Semiconductor, Kyoto, Japan, 2016, pp. 1–4.

[37] *CoreLossCalculation2017.pdf*. Accessed: Jan. 2020. [Online]. Available: https://www.maginc.com/getattachment/Design/Design-Guides/Powder-Core-Loss-Calculation/Powder-Core-Loss-Calculation.pdf?lang=en-US

[38] B. H. Carneiro, "Calculating and interpreting power dissipation for polypropylene film DC-link capacitors polypropylene film DC-link capacitors," Tech. Rep., 2017. Accessed: Jan. 2020. [Online]. Available: https://www.vishay.com/docs/26071/calcinterppowdisspolypfilmdcl.pdf

[39] *Gate Drive Voltage Recommendations for Wolfspeed 650 V 3rd Generation Silicon Carbide MOSFETs*, Wolfspeed, Durham, NC, USA, 2021, pp. 3–5.

MESHARI ALSHAMMARI received the B.Sc. degree in electrical engineering from the University of Hail, Saudi Arabia, in 2014, and the M.E. degree in energy systems engineering and the Ph.D. degree in electrical and electronics engineering from the University of Galway, in 2017 and 2022, respectively. He is currently a Senior Lecturer at the Electrical Engineering Department, Al Jouf University, Sakaka, Saudi Arabia. His research interests include the analysis of AC and DC building distribution systems, DC/AC power converters for utility grid applications, and renewable energy applications. In addition, he was awarded the best poster at the seventh NUI Galway Research Day, in 2017, and Best Paper at ICRERA 2021.

MAEVE DUFFY (Senior Member, IEEE) received the Ph.D. degree in electronic engineering in the area of power electronics from the National University of Ireland, Galway, in 1997. From 1997 to 2001, she worked with the PEI Technologies Group, NMRC (currently Tyndall Institute), Cork. While there, she participated in several EU and industry funded projects; her work involved the development of circuit models for integrated magnetic components formed in different microfabrication technologies. Since 2001, she has been lecturing in electrical and electronic engineering at the University of Galway. She is also carrying out research with the Power Electronics Research Centre. Her research interests include integrated and planar magnetics, including power electronic applications, such as VRM inductors, energy harvesting, and wireless power systems. She has extensive experience in finite element analysis modeling of magnetic components.

• • •